Nondipole ionization dynamics in atoms induced by intense xuv laser fields

Morten Førre* and Aleksander Skjerlie Simonsen†
Department of Physics and Technology, University of Bergen, N-5007 Bergen, Norway
(Received 25 September 2014; published 10 November 2014)

Solving the time-dependent Schrödinger equation from first principles, the laser-induced breakup dynamics of hydrogen is studied beyond the electric dipole approximation, at very high laser intensities. It is assumed that the atom is being irradiated by an extreme ultraviolet laser light pulse at a wavelength of 13 nm, corresponding to a photon energy of 95 eV. It has already been experimentally demonstrated that the free-electron laser (FEL) FLASH in Hamburg can deliver irradiance levels up to about 10^{16} W/cm^2 in this wavelength range. Although we will go to even higher intensities in the present work, in order to spot nondipole effects, this merely demonstrates that ultrahigh light intensities can be achieved with present FEL technologies. Furthermore, with new seeding techniques the laser power is expected to go even higher in the future. In our study the atom is exposed to a short attosecond laser pulse, and the role of higher-order corrections to the electric dipole approximation is studied systematically. The main findings are that higher-order corrections beyond the leading first-order term, to a good approximation, can be neglected for all intensities within the nonrelativistic regime, provided the pulse duration is not too long. This means that the effect of second- and higher-order corrections only needs to be accounted for when entering the relativistic regime, within the scope of the Dirac equation. It is further found that the leading first-order correction to the dipole approximation has a great impact on the angular emission pattern of the low-energy photoelectrons.

DOI: 10.1103/PhysRevA.90.053411 PACS number(s): 32.80.Rm, 42.50.Hz, 32.80.Fb

I. INTRODUCTION

The interaction between atoms and laser fields is of fundamental interest and has occupied physicists since the invention of the laser in 1960. Laser pulses are today by far the most powerful tools for manipulating and controlling atomic systems and have opened a new era in the field of atomic, molecular, and optical (AMO) physics. With the development of ultrashort (femtosecond) pulses, the possibility of using lasers as a kind of advanced camera for watching chemical reactions in real time has become a reality [1]. The invention of attosecond pulses through high-order harmonic generation (HHG) techniques [2,3] has brought the study of atomic processes to a new level of complexity [4], opening the door for generating extremely short laser pulses of durations comparable to the electron's (classical) orbit time in atoms, opening up new perspectives in imaging technologies. Free-electron lasers represent another laser technology that is developed in parallel with HHG sources [5,6]. Radiation produced by FEL is characterized by its high photon energies and high intensity, thus enabling the study of nonlinear breakup processes [7–9] as well as *K*-shell ionization followed by Auger decay [10]. With new seeding techniques the peak brightness and coherence properties of FELs are expected to improve even more in the future.

One of the most common approximations in AMO physics is to treat the laser field as a homogeneous time-dependent electric field, i.e., the so-called electric dipole approximation. In this approximation any spatial dependence of the fields as well as the homogeneous magnetic field component are assumed to be negligible. As a matter of fact, the dipole approximation is usually a very accurate one, and it is only under certain circumstances that nondipole corrections need to be considered, e.g., for very intense laser fields. Above-threshold ionization (ATI) and HHG by near-infrared light beyond the electric dipole approximation have been studied in atoms [11,12], and the breakdown of the dipole approximation in high-order harmonic generation in molecules has been demonstrated [13,14], i.e., both even and odd harmonics are obtained beyond the dipole approximation. Near the cutoff and for high intensities, it was shown that the even harmonic generation originating from the nondipole component of the driving field may ultimately become the dominating source of HHG in polyacetylene [13]. The role of nondipole effects in the ionization of hydrogen in superintense xuv laser pulses has also been investigated [15–20] within the context of atomic stabilization [21,22]. A characteristic lobe, coined the nondipole lobe, was recognized in the corresponding angular distribution of the emitted photoelectron [23,24], a finding that was confirmed more recently [25]. A similar lobe was also identified in the intense-field ionization of H_2^+ [26]. Furthermore, the electric dipole approximation is not applicable in the extremely short-wavelength limit, e.g., in the photoionization of atoms by hard x-ray radiation [27–31].

The aim of the present work is to study the breakdown of the electric dipole approximation in the multiphoton ionization dynamics of atoms in intense laser fields. We will consider the soft x-ray regime, i.e., the photon energy 95 eV, corresponding to a laser wavelength of 13 nm. This particular choice is motivated by the availability of such photons at the European free-electron laser facility at DESY in Hamburg (FLASH). FLASH can deliver irradiance levels up to about 10^{16} W/cm^2 at the current photon energy [7], and even higher intensities are expected with future seeding techniques [5,32]. In this work, we show that higher-order corrections to the electric dipole approximation, beyond the leading first-order nondipole correction, which corresponds to the (homogeneous) magnetic field component of the laser field, only have a minor effect on the resulting ionization dynamics and can under most

*morten.forre@ift.uib.no
†aleksander.simonsen@ift.uib.no

circumstances be neglected. In order to show this, we solve the fully three-dimensional time-dependent Schrödinger equation (TDSE) for a hydrogen atom interacting with an explicitly time- and space-dependent laser field, and obtain both total as well as differential ionization probabilities. At high intensities, the ionization dynamics is characterized by the emission of low-energy electrons, giving rise to a low-energy structure in the energy spectrum of the photoelectron. As this is a kind of high-frequency counterpart to the well established low-energy structure (LES) [33–35] observed in strong-field ionization of atoms and molecules by midinfrared laser fields, we merely call it the high-frequency low-energy structure (HLES) here. The HLES has been noticed before [19,36]. Here, we show that the emission of low-energy electrons becomes even more important in the nondipole limit, as the relative fraction of low-energy electrons that are emitted increases significantly. Furthermore, we show that the corresponding angular distributions of the low-energy electrons are significantly altered by the nondipole (homogeneous magnetic field) component of the laser field.

Our results are valid in the entire nonrelativistic domain, i.e., for all field strengths so that the corresponding quiver velocity of a (classical) free electron in the field does not exceed 10% of the speed of light. For even higher laser intensities, the nonrelativistic TDSE approach cannot be applied, our results are no longer valid, and a fully relativistic approach is a prerequisite for treating the problem [37–39].

Atomic units where m_e, $\hbar$, e, and a_0 are scaled to unity are used throughout the paper unless stated otherwise.

II. THEORY AND METHODOLOGY

Assuming the dynamics of the laser-atom interaction being nonrelativistic, the dynamics of a hydrogen atom interacting with a classical electromagnetic field is governed by the time-dependent Schrödinger equation, which in the velocity gauge is given by

$$i\frac{\partial}{\partial t}\Psi(\boldsymbol{r},t) = H\Psi(\boldsymbol{r},t), \tag{1}$$

with the Hamiltonian

$$H = \frac{1}{2}[\boldsymbol{p} + \boldsymbol{A}(\eta)]^2 - \frac{1}{r}. \tag{2}$$

Here $\boldsymbol{A}(\eta)$ is the time- and space-dependent vector potential defining the laser pulse, $\eta = \omega t - \boldsymbol{\kappa}\cdot\boldsymbol{r}$, ω is the central frequency of the field, $\kappa = |\boldsymbol{\kappa}| = \omega/c$ is the wave number, c is the speed of light, and $r = |\boldsymbol{r}|$. Assuming light propagating in the positive x direction and of linear polarization along the z axis, and expanding the space-dependent vector potential to second order in powers of x/c, the vector potential takes the approximate form

$$A(x,t) \simeq A(t) + \frac{x}{c}E(t) - \frac{1}{2}\frac{x^2}{c^2}\frac{d}{dt}E(t), \tag{3}$$

where $A(t)$ represents the homogeneous z component of the vector potential, and $E(t) = -\frac{d}{dt}A(t)$ is the corresponding (homogeneous) electric field. In the present work, we have assumed a sine-squared carrier envelope for the laser pulse, i.e., the time variation of the corresponding vector potential follows

$$A(t) = \frac{E_0}{\omega}\sin^2\left(\frac{\pi t}{T}\right)\sin(\omega t + \phi), \tag{4}$$

where E_0 is the maximum electric field amplitude, ϕ is the carrier-envelope phase (CEP), and T defines the (total) duration of the laser pulse. In the simulations, the CEP is set to zero and the pulse duration is given in numbers of optical cycles. As the laser pulse considered here is relatively long in terms of optical cycles, i.e., 15 cycles or longer, the actual value of the CEP is rather unimportant for the results.

Inserting the vector potential in Eq. (3) into the Hamiltonian Eq. (2), and imposing the Coulomb gauge restriction $\boldsymbol{\nabla}\cdot\boldsymbol{A} = 0$ on the field, we define three approximate Hamiltonians for the laser-matter interaction: first, the usual dipole approximation Hamiltonian,

$$H_{\mathrm{D}} \simeq \frac{1}{2}p^2 - \frac{1}{r} + A(t)p_z, \tag{5}$$

second, the Hamiltonian including the leading-order nondipole correction,

$$H_{\mathrm{ND}_1} \simeq \frac{1}{2}p^2 - \frac{1}{r} + A(t)p_z + \frac{x}{c}A(t)E(t), \tag{6}$$

and third, the Hamiltonian including also the next-leading-order nondipole corrections, which we also will refer to as the second-order nondipole corrections,

$$H_{\mathrm{ND}_2} \simeq \frac{1}{2}p^2 - \frac{1}{r} + \left[A(t) + \frac{x}{c}E(t)\right]p_z + \frac{x}{c}A(t)E(t) + \frac{1}{2}\frac{x^2}{c^2}\left[E^2(t) - A(t)\frac{d}{dt}E(t)\right]. \tag{7}$$

Note that here the purely time-dependent quadratic $\frac{1}{2}A^2(t)$ term has been removed by the gauge transformation

$$\Psi' = \exp\left[i\int_0^t \frac{1}{2}A^2(t')dt'\right]\Psi. \tag{8}$$

The difference between Eqs. (6) and (7) is that in Eq. (6) only the leading-order nondipole correction is included in addition to the dipole term, whereas in Eq. (7) the next-leading-order corrections are included as well. Note that we have here chosen to not follow the usual convention of including or excluding terms in the expansion of the Hamiltonian depending on their inverse powers of c, as seen in Eqs. (6) and (7), but rather to add or omit terms depending of their physical significance. To elaborate on this, assuming for the moment that the laser field is monochromatic, i.e., $A(t) = E_0/\omega\sin(\omega t)$, the time variation of the individual components of the interaction Hamiltonian (7) follows

$$A(t)p_z = \frac{E_0}{\omega}\sin(\omega t)p_z \tag{9}$$

$$\frac{x}{c}E(t)p_z = -\frac{x}{c}E_0\cos(\omega t)p_z \tag{10}$$

$$\frac{x}{c}A(t)E(t) = -\frac{1}{2}\frac{x}{c}\frac{E_0^2}{\omega}\sin(2\omega t) \tag{11}$$

$$\frac{1}{2}\frac{x^2}{c^2}\left[E^2(t) - A(t)\frac{d}{dt}E(t)\right] = \frac{1}{2}\frac{x^2}{c^2}E_0^2\cos(2\omega t). \tag{12}$$

Including yet higher-order corrections into the Hamiltonian (7) would also yield terms oscillating with either ω or 2ω. This is a consequence of the fact that the full interaction Hamiltonian (2) contains two kind of operators for the atom-field interaction, i.e., the $\boldsymbol{A}\cdot\boldsymbol{p}$ and $\boldsymbol{A}^2/2$ operators, representing one and two-photon transitions, respectively. As such, the $x/cA(t)E(t)$ operator is not merely a correction to the electric field component already included in the dipole approximation, but represents two-photon transitions associated with the radiation pressure caused by the combined (homogeneous) electric and magnetic fields. Radiation pressure is not accounted for in the dipole approximation due to the complete absence of a magnetic field component. The $\boldsymbol{A}^2/2$ operator does not contribute to the dynamics within the dipole approximation, as the transformation (8) cancels out its effect, and we therefore consider its first-order component $x/cA(t)E(t)$ to be the leading-order term in its own right. Hence, the xp_z and the x^2 operators merely represent the first-order corrections to the two leading-order terms (9) and (11), respectively, and as a result they should either both be included or omitted from the interaction Hamiltonian, cf. Eqs. (7) and (6). These corrections arise due to the spatial expansion of the electromagnetic field and are expected to become important for the ionization dynamics in the regime of extremely high-frequency fields or for very long pulses. In our case, the additional terms in Eq. (7) are of equal significance to the nondipole dynamics, despite the different inverse powers in c. This can perhaps be understood from the fact that they both account for the first-order spatial correction but to the two different types of transitions.

The numerical problem at hand is extremely challenging in terms of convergence properties. The origin of the numerical difficulty stems from the additional terms in Eq. (7) and the diverse selection rules of the corresponding operators [see Eqs. (A8) and (A9) in the Appendix]. Here, the different components of the operators, that can be associated with a given selection rule, happen to have great impact on the numerics individually, but the net effect when all components are combined together may still be small. This might cause what is known as catastrophic cancellation, and therefore extra caution is needed when handling the problem numerically. With this in mind, and in order to be confident in the results, we have pursued two independent numerical approaches.

In the first approach, the time-dependent wave function is expanded in B-spline functions [40] for the radial coordinate and spherical harmonics for the angular components,

$$\Psi(\mathbf{r},t)=\sum_{klm}c_{klm}(t)\frac{B_k(r)}{r}Y_{lm}(\theta,\phi). \tag{13}$$

Here m runs from $-l$ to l, l runs from 0 to an upper value $l_{\max}$, and $B_k(r)$ is the kth B-spline function. We distribute the B-spline functions equidistantly in a radial box limited at the largest value $R_{\max}$. B-spline functions do not have the property of being orthogonal, but they have compact support, i.e., they are nonzero only on some finite interval [40]. As such, any operator constructed in a B-spline-based expansion will be sparse in a matrix representation. This is one of the main advantages of solving the TDSE directly in a B-spline-based basis, as matrix-vector products are numerically cheap when only operating upon nonzero entries, and memory consumption is significantly reduced as compared to a representation with global basis functions such as atomic eigenstates. However, the use of B splines poses some restrictions on the choice of time-propagation scheme, as the system becomes a so-called stiff problem [41]. Therefore, we apply an unconditionally stable temporal integration method, i.e., an implicit scheme. Here, we make use of the Cayley propagator, also known as the Crank-Nicholson scheme, which relates the wave function one step into the future, $\Psi(t+\Delta t)$, to the current wave function, $\Psi(t)$, as

$$\left(S+\frac{i\Delta t}{2}H(t+\Delta t)\right)\Psi(\mathbf{r},t+\Delta t)=\left(S-\frac{i\Delta t}{2}H(t)\right)\Psi(\mathbf{r},t), \tag{14}$$

where S is the basis overlap matrix, made necessary by the nonorthogonality of the B-spline basis functions,

$$S_{klm,k'l'm'}=\delta_{l,l'}\delta_{m,m'}\int B_k(r)B_{k'}(r)dr. \tag{15}$$

Equation (14) has the property of being numerically stable for stiff problems, but comes with the price of requiring the application of a linear solver in every time step. The time step Δt should in addition be kept small in order to minimize the truncation error.

When applying the wave function expansion in Eq. (13) to the Hamiltonian Eqs. (5)–(7), the resulting Hamiltonian matrix may acquire a large dimension. As such, applying a linear solver, as made necessary by Eq. (14), is unpractical for the standard algorithms due to the cubic scaling of arithmetical operations with the number of unknowns. Instead, an iterative linear solver based on a Krylov subspace expansion is used. Such a solver can exploit the sparse structure of the matrix, as its kernel requires only matrix-vector products. We solve the systems of equations (14) with the generalized minimal residual (GMRES) algorithm [42]. Due to the ill-conditioned nature of the atomic Hamiltonian matrix, straightforward application of the GMRES algorithm results in poor convergence. This is remedied by first applying an incomplete LU algorithm (a preconditioner), solving only the time-independent parts of the left-hand matrix of Eq. (14). Since the preconditioner is time independent, the incomplete factorization is performed only once prior to the propagation, and each time step necessitates a combination of a forward and a backward substitution of a banded sparse matrix. The technique is numerically cheap, due to the sparse nature of the system, and it significantly increases the convergence rate of the GMRES. When applying the preconditioner, the GMRES algorithm typically converges within a few tens of iterations. The core and time-consuming component of the algorithm depends exclusively upon matrix-vector products, and as such, the computations can conveniently be distributed on an arbitrary number of processors in a distributed-memory architecture.

In the second numerical approach to solve the TDSE, we have expanded the time-dependent wave function in

time-independent eigenstates as

$$\Psi(\mathbf{r},t) = \sum_{klm} c_{klm}(t)\psi_{klm}(r,\theta,\phi)$$
$$= \sum_{klm} c_{klm}(t)R_{kl(r)}Y_{lm}(\theta,\phi)$$
$$= \sum_{klm} c_{klm}(t)\frac{u_{kl}(r)}{r}Y_{lm}(\theta,\phi), \quad (16)$$

where $R_{kl}(r)$ is the radial wave function (including both continuum and bound states) of the hydrogen atom and $u_{kl}(r) = rR_{kl}(r)$ is the corresponding reduced radial wave function. The radial wave functions are obtained by diagonalizing the field-free Hamiltonian in a B-spline basis. Then, the dipole and nondipole coupling elements are calculated using the relations given in the Appendix and the resulting system of ordinary differential equations are solved by a predictor-corrector method developed by Shampine and Gordon [43].

The two numerical representations (13) and (16) have both their advantages and disadvantages. The B-spline-based approach has the clear advantage that it can be applied to much larger numerical problems (higher $l_{\max}$), simply due to the sparseness of the resulting matrices and the following low-cost memory consumption. On the other hand, the eigenstate approach is significantly more well conditioned and the predictor-corrector method is implemented with an adaptive time step that controls the truncation error. To this end, as a means to control the numerical convergence of the results, both numerical approaches have been pursued in the present work.

Having obtained the final wave function at the end of the laser pulse, the resulting angular- and energy-resolved probability density is obtained as

$$\frac{d^2P}{dkd\Omega} = \left|\sum_{lm}(-i)^l e^{i\sigma_l}Y_{lm}(\Omega)\left\langle\Phi^C_{klm}(\boldsymbol{r})\middle|\Psi(\boldsymbol{r},t=T)\right\rangle\right|^2, \quad (17)$$

where $\Psi(\boldsymbol{r},t=T)$ is the wave function at the end of the pulse, $\Phi^C_{klm}(\boldsymbol{r})$ is the Coulomb wave function (normalized on the k scale), $k = \sqrt{2E}$ is the wave number, and $\sigma_l = \arg\Gamma(l+1-i/k)$ is the Coulomb phase shift.

III. RESULTS AND DISCUSSION

We find that the problem at hand is quite demanding in terms of computational resources. During the laser-atom interaction the electron attains a high value of angular momentum. As a matter of fact, $l_{\max} = 69$ is required in order to obtain fully converged results. This makes the total number of angular channels 4900 when all values of the magnetic quantum number, m, are explicitly included. With roughly a thousand B splines the dimension of the problem is of the order of 5×10^6. The B splines are distributed in a radial box extending to $R_{\max} = 300$ a.u., making sure that the (ionized) wave function can evolve freely into the space exterior to the atom during the laser-atom interaction.

Figure 1 shows the total ionization probability as a function of the peak electric field amplitude of the laser pulse, for a pulse of 15 cycle duration and angular frequency $\omega =$ 3.5 a.u., corresponding to 95 eV photons. Results obtained by solving the TDSE with the three Hamiltonian Eqs. (5)–(7) are shown for comparison. It is seen that, as far as the total ionization probability is concerned, the electric dipole approximation breaks down at about $E_0 = 30$ a.u. for the laser parameters considered. Furthermore, the results applying the Hamiltonians (6) and (7) are virtually identical. As a matter of fact, it is found that the difference in total ionization yield is less than 0.5% for all intensities considered. This means that the Hamiltonian in Eq. (6) turns out to be a good approximation to the dynamics as far as the total survival probability is concerned. A similar conclusion was drawn in a previous study of nondipole effects in a two-dimensional model atom [15,16]. The decrease in the ionization probability with increasing laser intensity, observed for the intermediate field strengths in Fig. 1, is a characteristic of the phenomenon called atomic stabilization [21,22]. The figure shows that the nondipole corrections have a detrimental effect on the degree of stabilization of the atom, in that the probability of ionization is enhanced, a result that is in agreement with earlier findings [15–20].

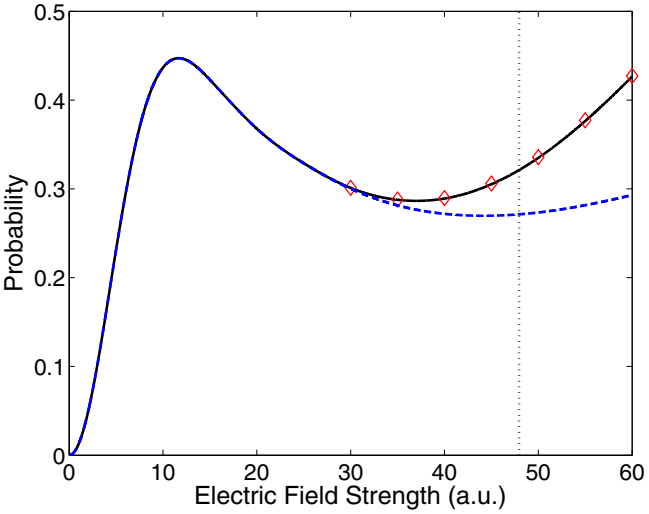

FIG. 1. (Color online) Total ionization probability vs electric field strength for a 15-cycle laser pulse with $\omega = 3.5$ a.u. Solid black line: the nondipole result obtained by solving the TDSE with the Hamiltonian in Eq. (6). Red diamonds: the nondipole result obtained by solving the TDSE with the Hamiltonian in Eq. (7). Dashed blue line: the dipole approximation result obtained by solving the TDSE with the Hamiltonian in Eq. (5). The vertical black dotted line indicates the limiting value where the quiver velocity of a corresponding free (classical) electron in the laser field may exceed 10% of the speed of light during the pulse, and where relativistic effects may become important.

Having confirmed the validity of the Hamiltonian (6) in obtaining total ionization yields, we now turn to the problem of testing whether the higher-order nondipole correction terms in Eq. (7) also can be neglected when calculating differential ionization probabilities. Figure 2 depicts the kinetic energy distribution of the photoelectron for the laser pulse considered in Fig. 1 and for three different laser intensities, $E_0 = 25$ a.u. (top panels), $E_0 = 35$ a.u. (middle panels), and $E_0 = 45$ a.u. (bottom panels). The left panels show a comparison between

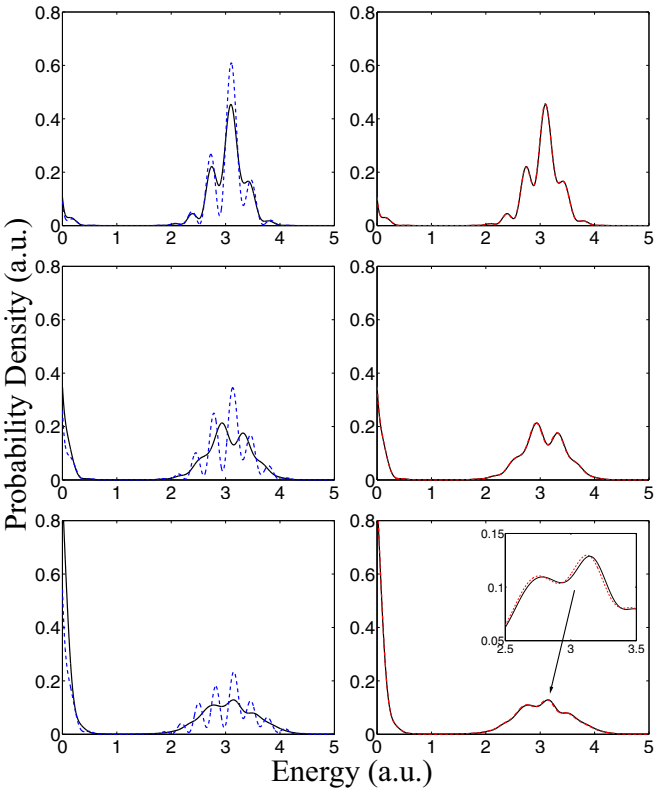

FIG. 2. (Color online) Kinetic energy spectrum of the emitted photoelectron for a 15-cycle laser pulse with $\omega = 3.5$ a.u., and for three different electric fields strengths, $E_0 = 25$ a.u. (top panels), $E_0 = 35$ a.u. (middle panels), and $E_0 = 45$ a.u. (bottom panels). Solid black line in left/right panels: the nondipole result obtained by solving the TDSE with the Hamiltonian in Eq. (6). Dashed blue line in left panels: the dipole approximation result obtained by solving the TDSE with the Hamiltonian in Eq. (5). Dashed red line in right panels: the nondipole result obtained by solving the TDSE with the Hamiltonian in Eq. (7).

the dipole approximation result (dashed blue line) and the result obtained with the nondipole Hamiltonian in Eq. (6) (solid black line). Likewise, the right panels depict the result obtained by solving the TDSE with the nondipole Hamiltonians Eqs. (6) (solid black line) and (7) (dashed red line), respectively.

The structure located around 3 a.u. of energy in Fig. 2 corresponds to the net absorption of one photon ($N = 1$) from the laser field. Starting with the left panels, clear differences are found between the dipole and nondipole spectra, in that the dipole result exhibits an oscillatory structure around the $N = 1$ resonance. The oscillations are also present in the nondipole calculations for the lower intensities, but are gradually washed out with increasing laser power. The oscillations are due to interferences caused by the multiple rescattering of the outgoing electron on the nucleus. Accordingly, the suppression of the oscillations in the nondipole limit is understood by the fact that the (nondipole) magnetic field component of the laser field, in combination with the electric (dipole) field, causes a radiation pressure on the electron in the laser propagation direction. As a result, the electron avoids the nucleus and multiple rescattering events become less likely, ultimately leading to the suppression of the interference fringes. It should be noted that, while nondipole effects are observed in the electron kinetic energy distribution even for the lowest laser field strength considered in Fig. 2, i.e., $E_0 = 25$ a.u., the dipole approximation result still provides the correct total ionization probability.

A structure located at low kinetic energies is also observed in Fig. 2. The structure becomes more pronounced for the highest intensities, and is present both in the dipole and nondipole cases. However, as it turns out, the emission of low-energy electrons is enhanced by nondipole effects, as can be clearly seen in the bottom left panel in the figure. The appearance of low-energy electrons in the high-frequency and high intensity limit was already discussed in earlier works [19,36], and was attributed to the nonadiabatic turn-on of the laser field and shake-off processes. The process may also be understood as a Λ- or Raman-type two-photon transition [22], where one photon is absorbed from the field while the other is emitted, the photon energy difference being transferred to the electron. Note that this type of process will be forbidden in the limit of monochromatic light, simply due to the energy conservation rule, but will be allowed in the case of short and intense laser fields. This also explains why the fraction of low-energy electrons increases with the laser pulse intensity in Fig. 2.

Turning to the right panels in Fig. 2, it is seen that the low-energy structure is essentially unaffected by the inclusion of second-order nondipole corrections. Nonetheless, a small difference between the results obtained by solving the TDSE with the Hamiltonians (6) and (7) is noticeable at the $N = 1$ resonance, in particular for the highest intensity. The inset in the bottom right panel reveals a small shift of the spectrum when including second-order nondipole effects. For even higher photoelectron energies, this trend becomes even more salient, as is demonstrated in Fig. 3. Figure 3 is an extension of Fig. 2 (bottom right panel), showing on a logarithmic scale the resonances corresponding to the net absorption of one, two, three, and four photons from the field, for $E_0 = 45$ a.u. As apparent from the figure, the induced shift, that is associated

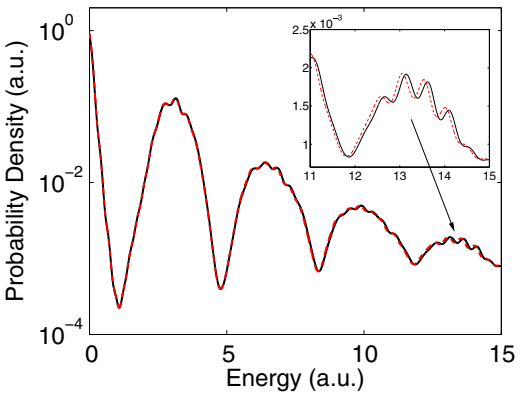

FIG. 3. (Color online) Kinetic energy spectrum of the emitted photoelectron for a 15-cycle laser pulse with $\omega = 3.5$ a.u., and for $E_0 = 45$ a.u. Solid black line: the nondipole result obtained by solving the TDSE with the Hamiltonian in Eq. (6). Dashed red line: the nondipole result obtained by solving the TDSE with the Hamiltonian in Eq. (7).

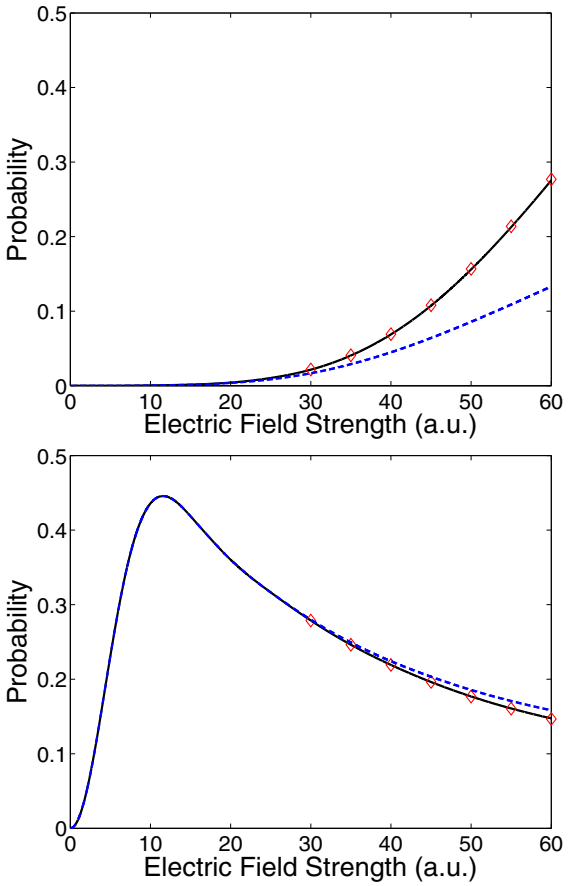

FIG. 4. (Color online) Ionization probability vs electric field strength for a 15-cycle laser pulse with $\omega = 3.5$ a.u. Top panel: total probability of emission of low-energy electrons, i.e., electron kinetic energy < 1 a.u. Bottom panel: total probability of emission of high-energy electrons, i.e., electron kinetic energy $E > 1$ a.u. Solid black line: the nondipole result obtained by solving the TDSE with the Hamiltonian in Eq. (6). Red diamonds: the nondipole result obtained by solving the TDSE with the Hamiltonian in Eq. (7). Dashed blue line: the dipole approximation result obtained by solving the TDSE with the Hamiltonian in Eq. (5).

with both the xp_z and x^2 nondipole terms in Eq. (7), increases with increasing kinetic energy of the continuum electron.

In Fig. 2 we observed that the emission of low-energy electrons became more important in the beyond dipole limit. To study this in more detail, the top panel in Fig. 4 shows the total probability of emission of low-energy electrons, i.e., electrons with energy less than 1 a.u., as a function of laser field strength. Likewise, the bottom panel in the figure depicts the corresponding probability for the emission of electrons with energies greater than 1 a.u., i.e., the probability for the net absorption of one, two, three, etc. photons from the field. Now it becomes clear that the likelihood of generating high-energy continuum electrons is largely unaffected by nondipole effects, and that the main nondipole effect sets in at low electron energies, leading to a decreased survival probability. Furthermore, the results in Fig. 4 confirm that the Hamiltonian (6) is a good approximation to the full nondipole dynamics. Comparing Figs. 1 and 4 it seems obvious that,

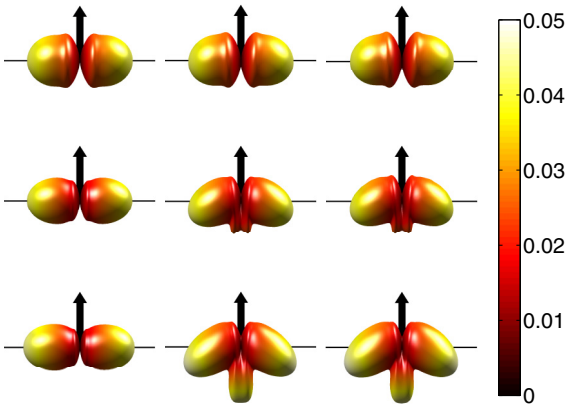

FIG. 5. (Color online) Electron angular distributions, integrated over electron energy, for $\omega = 3.5$ a.u., and for a 15-cycle laser pulse linearly polarized in the horizontal direction and propagating in the upward direction (indicated with an arrow), and for three different electric field strengths, $E_0 = 30$ a.u. (top panels), $E_0 = 40$ a.u. (middle panels), and $E_0 = 45$ a.u. (bottom panels). Left column: the dipole approximation result obtained by solving the TDSE with the Hamiltonian in Eq. (5). Middle column: the nondipole result obtained by solving the TDSE with the Hamiltonian in Eq. (6). Right column: the nondipole result obtained by solving the TDSE with the Hamiltonian in Eq. (7).

in the context of atomic stabilization [15–22], if one were to measure the stabilizing effect experimentally, it would be advantageous to design the experiment (the laser pulse) so that the production of low-energy electrons is suppressed.

The angular distributions of the continuum electron is plotted in Fig. 5. The data are taken for a 15-cycle laser pulse with $\omega = 3.5$ a.u., and for $E_0 = 30$ (top panels), 40 (middle panels), and 45 a.u. (bottom panels), respectively. The horizontal axis in the figure indicates the laser polarization direction, and the pulse propagates in the upward direction, as shown by the arrow. The dipole result is depicted in the left column, and the nondipole results obtained with the Hamiltonians (6) and (7) are presented in the middle and right columns, respectively. Obviously, the nondipole Hamiltonian (6) again yields very accurate results, as no visible difference between the two nondipole calculations is detected. For the lowest laser intensity ($E_0 = 30$ a.u.) the dipole approximation result is valid, whereas for the two higher intensities clear nondipole effects are expressed, the main one being a characteristic angular lobe growing along the counterpropagating direction (downward in the figure). The emergence of this unique nondipole lobe in the angular distributions, as well as the mechanism behind it, have been discussed in previous works [23–26,39], and is related to the radiation pressure of the combined (homogeneous) electric and magnetic fields acting on the electron throughout the laser pulse [23]. This leads to a net shift of the electronic wave function in the laser propagation direction, from which the electron falls in the bare Coulomb field of the atomic nucleus as the laser pulse deceases and scatters off it. The bending of the two other lobes pointing along the laser polarization axis was also discussed in Ref. [23] and arises from a similar mechanism.

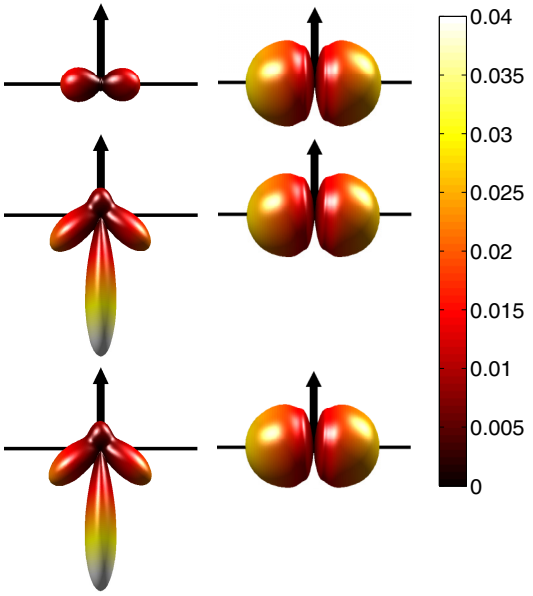

FIG. 6. (Color online) Electron angular distributions, integrated over electron energy, for $\omega = 3.5$ a.u., $E_0 = 45$ a.u., and for a 15-cycle laser pulse linearly polarized in the horizontal direction and propagating in the upward direction (indicated with an arrow). Left column: the angular distribution of the low-energy electrons, i.e., electron kinetic energy < 1 a.u. Right column: the angular distribution of the high-energy electrons, i.e., electron kinetic energy $E > 1$ a.u. Top panels: the dipole approximation result obtained by solving the TDSE with the Hamiltonian in Eq. (5). Middle panels: the nondipole result obtained by solving the TDSE with the Hamiltonian in Eq. (6). Bottom panels: the nondipole result obtained by solving the TDSE with the Hamiltonian in Eq. (7).

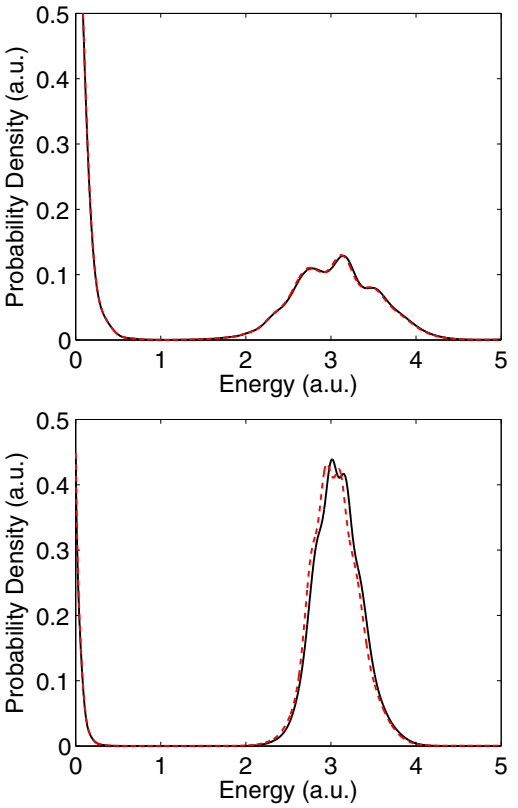

FIG. 7. (Color online) Kinetic energy spectrum of the emitted photoelectron for $\omega = 3.5$ a.u. and $E_0 = 45$ a.u. Top panel: 15-cycle laser pulse. Bottom panel: 30-cycle laser pulse. Solid black line: nondipole result obtained by solving the TDSE with the Hamiltonian in Eq. (6). Dashed red line: nondipole result obtained by solving the TDSE with the Hamiltonian in Eq. (7).

The left column in Fig. 6 shows the angular distribution emerging from the low-energy electrons solely, i.e., from electrons having kinetic energies less than 1 a.u. Correspondingly, the right column depicts the distribution attributed to electrons with energies higher than 1 a.u. The top panel yields the dipole result, while middle and bottom panels present the nondipole calculations with the Hamiltonians (6) and (7), respectively. Only the result for $E_0 = 45$ a.u. is shown in the figure, and the pulse is the same as before. As can be seen from the figure, the angular distributions of the high-energy electrons are largely unaffected by nondipole effects, while the bending of the lobes as well as the extra nondipole lobe emerge from the low-energy electrons.

We have found that the emergence of low-energy electrons in the ionization process is intimately related to the nonadiabatic turn-on of the laser pulse and shake-off processes, in particular in the dipole approximation case. In the nondipole limit, production of low-energy electrons is enhanced due to the electron-nucleus scattering process during the laser pulse ramp-off. Furthermore, as it turns out higher-order nondipole corrections beyond the leading first-order correction are essentially unimportant for the relatively short laser pulse (15 cycles) considered, the only observed difference being a minor shift of the multiphoton peaks in the corresponding kinetic energy distributions of the photoelectron, cf. Fig. 3. Now, the natural question arises as to what will happen in the long-pulse duration limit; can higher-order nondipole corrections to the laser field still be neglected? Such a question is also interesting from the point of view of FELs, as FEL pulses typically have durations of the order of femtoseconds, as opposed to the attosecond pulse considered here. In order to seek an answer to such question, we have considered a laser pulse twice as long.

Figure 7 presents a comparison of the kinetic energy spectrum of the photoelectron for $\omega = 3.5$ a.u. and $E_0 = 45$ a.u., for a 15-cycle (top panel) and 30-cycle (bottom panel) laser pulse, respectively. The figure reveals two characteristic features: First, the fraction of low-energy electrons declines for the longer pulse, as the laser turn-on and turn-off becomes more adiabatic. But more importantly, the role of the higher-order nondipole correction terms in the Hamiltonian (7) clearly becomes more important for the longer pulse, in that the photon resonance corresponding to the net absorption of one photon from the field is shifted to lower electron energies when second-order corrections are considered. The corresponding shift is much less pronounced for the shorter pulse (top panel in the figure). This merely demonstrates that, despite higher-order nondipole corrections are of less importance to the nondipole dynamics, they still come into play in the long pulse regime. Nevertheless, we have found that the total ionization probability is much less influenced

by second-order nondipole effects, the difference between the results obtained with the Hamiltonians (6) and (7) being only about one percent in the present case. For the 30-cycle pulse, the corresponding ionization probabilities are 0.409 and 0.404, respectively.

IV. CONCLUSION AND SUMMARY

In summary, we have studied atomic hydrogen exposed to ultrashort intense 13 nm laser light in the nondipole regime. We have solved the time-dependent Schrödinger equation from first principles in three dimensions. Three separate laser-atom interactions have been considered: the electric dipole approximation, the first-order nondipole correction to the dipole approximation, and finally, the interaction including both first- and second-order nondipole corrections. Among all nondipole corrections considered, the radiation pressure caused by the addition of the homogeneous magnetic field component to the laser field is found to be the most important one. Its contribution is manifested as a characteristic lobe in the photoelectron angular distribution [23]. Also, the kinetic energy distributions of the ionized electrons show that the magnetic field component has a tendency to suppress rescattering events between the outgoing electron and the nucleus. A more detailed analysis reveals that most electrons emitted due to nondipole ionization dynamics are emitted with extremely low kinetic energy and that the previously discovered nondipole lobe in the angular distributions comprises such low-energy electrons. We find that, while the second-order (spatial) nondipole corrections bring additional complexity and numerical difficulties to the problem, they contribute very little to the ionization dynamics in the present case. The small effect observed is characterized by a tiny shift in the photoelectron kinetic energy distribution, where the spatial dependencies included in the fields cause emission of slightly less energetic electrons. It is further found that the shift becomes more salient for longer pulse durations.

ACKNOWLEDGMENTS

This work was supported by the Bergen Research Foundation and the Norwegian Metacenter for Computational Science (Notur). Calculations were performed on the Cray XE6 (Hexagon) supercomputer installation at Parallab, University of Bergen (Norway).

APPENDIX

Expanding a (general) one-electron wave function in hydrogenic radial wave functions for the radial part and spherical harmonics for the angular parts, cf. Eq. (16), the matrix elements of the corresponding Hamiltonian $\hat{H}$ are formally given by

$$\begin{aligned}\langle\psi_{klm}|\hat{H}|\psi_{k'l'm'}\rangle &= \langle R_{kl}Y_{lm}|\hat{H}|R_{k'l'}Y_{l'm'}\rangle \\ &= \left\langle \frac{u_{kl}}{r}Y_{lm}\middle|\hat{H}\middle|\frac{u_{k'l'}}{r}Y_{l'm'}\right\rangle,\end{aligned} \tag{A1}$$

where $u_{kl}(r) = rR_{kl}(r)$ is the reduced radial wave function. In deriving the matrix elements of the Hamiltonians (5)–(7), we have made use of the following relations for the spherical harmonics:

$$\begin{aligned}\sin\theta\cos\phi Y_{lm} &= -a_{lm}Y_{l-1,m-1} + a_{l,-m}Y_{l-1,m+1} \\ &\quad + a_{l+1,-m+1}Y_{l+1,m-1} - a_{l+1,m+1}Y_{l+1,m+1}\end{aligned} \tag{A2}$$

$$\cos\theta Y_{lm} = b_{l+1,m}Y_{l+1,m} + b_{lm}Y_{l-1,m} \tag{A3}$$

$$\begin{aligned}\sin\theta\frac{\partial}{\partial\theta}Y_{lm} &= lb_{l+1,m}Y_{l+1,m} - (l+1)b_{lm}Y_{l-1,m} \\ a_{lm} &= \sqrt{\frac{(l+m)(l+m-1)}{4(2l-1)(2l+1)}} \\ b_{lm} &= \sqrt{\frac{l^2-m^2}{(2l-1)(2l+1)}}.\end{aligned} \tag{A4}$$

Then,

$$\begin{aligned}\frac{\partial}{\partial z}\left(\frac{u_{kl}}{r}Y_{lm}\right) &= \left(\cos\theta\frac{\partial}{\partial r} - \frac{1}{r}\sin\theta\frac{\partial}{\partial\theta}\right)\left(\frac{u_{kl}}{r}Y_{lm}\right) \\ &= \left(\frac{1}{r}\frac{du_{kl}}{dr} - \frac{l+1}{r^2}u_{kl}\right)b_{l+1,m}Y_{l+1,m} \\ &\quad + \left(\frac{1}{r}\frac{du_{kl}}{dr} + \frac{l}{r^2}u_{kl}\right)b_{lm}Y_{l-1,m},\end{aligned} \tag{A5}$$

and the nonzero matrix elements of the p_z operator becomes

$$\begin{aligned}\langle\psi_{klm}|p_z|\psi_{k'l'm'}\rangle &= -i\left\langle\frac{u_{kl}}{r}Y_{lm}\middle|\frac{\partial}{\partial z}\middle|\frac{u_{k'l'}}{r}Y_{l'm'}\right\rangle \\ &= -i\left\langle\frac{u_{kl}}{r}Y_{lm}\middle|\left(\frac{1}{r}\frac{du_{k'l'}}{dr} - \frac{l'+1}{r^2}u_{k'l'}\right)b_{l'+1,m'}Y_{l'+1,m'} + \left(\frac{1}{r}\frac{du_{k'l'}}{dr} + \frac{l'}{r^2}u_{k'l'}\right)b_{l'm'}Y_{l'-1,m'}\right\rangle \\ &= -ib_{lm}\delta_{l',l-1}\delta_{m',m}\int_0^\infty u_{kl}\left(\frac{du_{k',l-1}}{dr} - l\frac{u_{k',l-1}}{r}\right)dr - ib_{l+1,m}\delta_{l',l+1}\delta_{m',m} \\ &\quad \times\int_0^\infty u_{kl}\left(\frac{du_{k',l+1}}{dr} + (l+1)\frac{u_{k',l+1}}{r}\right)dr.\end{aligned} \tag{A6}$$

Using Eq. (A2), the nonzero matrix elements of the leading first-order nondipole correction, i.e., the x term in the nondipole Hamiltonians (6) and (7), take the form

$$\begin{aligned}\langle\psi_{klm}|x|\psi_{k'l'm'}\rangle &= \left\langle \frac{u_{kl}}{r}Y_{lm}\middle| r\sin\theta\cos\phi\middle|\frac{u_{k'l'}}{r}Y_{l'm'}\right\rangle \\ &= -a_{l+1,m+1}\delta_{l',l+1}\delta_{m',m+1}\int_0^\infty ru_{kl}u_{k',l+1}dr + a_{l+1,-m+1}\delta_{l',l+1}\delta_{m',m-1}\int_0^\infty ru_{kl}u_{k',l+1}dr \\ &\quad + a_{l,-m}\delta_{l',l-1}\delta_{m',m+1}\int_0^\infty ru_{kl}u_{k',l-1}dr - a_{lm}\delta_{l',l-1}\delta_{m',m-1}\int_0^\infty ru_{kl}u_{k',l-1}dr. \end{aligned} \tag{A7}$$

Applying the relation (A2) two times, the nonzero elements of the x^2 operator in Eq. (7) are given by

$$\begin{aligned}\langle\psi_{klm}|x^2|\psi_{k'l'm'}\rangle &= \left\langle \frac{u_{kl}}{r}Y_{lm}\middle| r^2\sin^2\theta\cos^2\phi\middle|\frac{u_{k'l'}}{r}Y_{l'm'}\right\rangle \\ &= a_{l+2,m+2}a_{l+1,m+1}\delta_{l',l+2}\delta_{m',m+2}\int_0^\infty r^2u_{kl}u_{k',l+2}dr \\ &\quad -(a_{l+2,m}a_{l+1,-m+1}+a_{l+2,-m}a_{l+1,m+1})\delta_{l',l+2}\delta_{m',m}\int_0^\infty r^2u_{kl}u_{k',l+2}dr \\ &\quad +a_{l+2,-m+2}a_{l+1,-m+1}\delta_{l',l+2}\delta_{m',m-2}\int_0^\infty r^2u_{kl}u_{k',l+2}dr \\ &\quad -(a_{l,m+2}a_{l,-m}+a_{l+1,-m-1}a_{l+1,m+1})\delta_{l',l}\delta_{m',m+2}\int_0^\infty r^2u_{kl}u_{k'l}dr \\ &\quad +(a_{lm}a_{lm}+a_{l,-m}a_{l,-m}+a_{l+1,-m+1}a_{l+1,-m+1} \\ &\quad +a_{l+1,m+1}a_{l+1,m+1})\delta_{l',l}\delta_{m',m}\int_0^\infty r^2u_{kl}u_{k'l}dr \\ &\quad -(a_{l,-m+2}a_{lm}+a_{l+1,m-1}a_{l+1,-m+1})\delta_{l',l}\delta_{m',m-2}\int_0^\infty r^2u_{kl}u_{k'l}dr \\ &\quad +a_{l-1,-m-1}a_{l,-m}\delta_{l',l-2}\delta_{m',m+2}\int_0^\infty r^2u_{kl}u_{k',l-2}dr \\ &\quad -(a_{l-1,-m+1}a_{lm}+a_{l-1,m+1}a_{l,-m})\delta_{l',l-2}\delta_{m',m}\int_0^\infty r^2u_{kl}u_{k',l-2}dr \\ &\quad +a_{l-1,m-1}a_{lm}\delta_{l',l-2}\delta_{m',m-2}\int_0^\infty r^2u_{kl}u_{k',l-2}dr. \end{aligned} \tag{A8}$$

Finally, using Eqs. (A2) and (A5) the nonzero matrix elements of the xp_z operator are calculated as

$$\begin{aligned}\langle\psi_{klm}|xp_z|\psi_{k'l'm'}\rangle &= -i\left\langle u_{kl}Y_{lm}\middle|x\middle|\left(\frac{1}{r}\frac{du_{k'l'}}{dr}-\frac{l'+1}{r^2}u_{k'l'}\right)b_{l'+1,m'}Y_{l'+1,m'}+\left(\frac{1}{r}\frac{du_{k'l'}}{dr}+\frac{l'}{r^2}u_{k'l'}\right)b_{l'm'}Y_{l'-1,m'}\right\rangle \\ &= ia_{l+1,m+1}b_{l+1,m+1}\delta_{l',l}\delta_{m',m+1}\int_0^\infty u_{kl}\left(r\frac{du_{k'l}}{dr}-(l+1)u_{k'l}\right)dr - ia_{l,-m}b_{l,m+1}\delta_{l',l}\delta_{m',m+1} \\ &\quad\times\int_0^\infty u_{kl}\left(r\frac{du_{k'l}}{dr}+lu_{k'l}\right)dr - ia_{l+1,-m+1}b_{l+2,m-1}\delta_{l',l+2}\delta_{m',m-1}\int_0^\infty u_{kl}\left(r\frac{du_{k',l+2}}{dr}+(l+2)u_{k',l+2}\right)dr \\ &\quad + ia_{l+1,m+1}b_{l+2,m+1}\delta_{l',l+2}\delta_{m',m+1}\int_0^\infty u_{kl}\left(r\frac{du_{k',l+2}}{dr}+(l+2)u_{k',l+2}\right)dr \\ &\quad + ia_{lm}b_{l-1,m-1}\delta_{l',l-2}\delta_{m',m-1}\int_0^\infty u_{kl}\left(r\frac{du_{k',l-2}}{dr}-(l-1)u_{k',l-2}\right)dr - ia_{l,-m}b_{l-1,m+1}\delta_{l',l-2}\delta_{m',m+1} \\ &\quad\times\int_0^\infty u_{kl}\left(r\frac{du_{k',l-2}}{dr}-(l-1)u_{k',l-2}\right)dr - ia_{l+1,-m+1}b_{l+1,m-1}\delta_{l',l}\delta_{m',m-1} \\ &\quad\times\int_0^\infty u_{kl}\left(r\frac{du_{k'l}}{dr}-(l+1)u_{k'l}\right)dr + ia_{lm}b_{l,m-1}\delta_{l',l}\delta_{m',m-1}\int_0^\infty u_{kl}\left(r\frac{du_{k'l}}{dr}+lu_{k'l}\right)dr. \end{aligned} \tag{A9}$$

[1] A. H. Zewail, Science **242**, 1645 (1988).
[2] M. Hentschel, R. Kienberger, C. Spielmann, G. A. Reider, N. Milosevic, T. Brabec, P. Corkum, U. Heinzmann, M. Drescher, and F. Krausz, Nature (London) **414**, 509 (2001).
[3] P. M. Paul, E. S. Toma, P. Breger, G. Mullot, F. Augé, P. Balcou, H. G. Muller, and P. Agostini, Science **292**, 1689 (2001).
[4] F. Krausz and M. Ivanov, Rev. Mod. Phys. **81**, 163 (2009).
[5] W. Ackermann *et al.*, Nature Photon. **1**, 336 (2007).
[6] T. Shintake *et al.*, Nature Photon. **2**, 555 (2008).
[7] A. A. Sorokin, S. V. Bobashev, T. Feigl, K. Tiedtke, H. Wabnitz, and M. Richter, Phys. Rev. Lett. **99**, 213002 (2007).
[8] G. Doumy, C. Roedig, S.-K. Son, C. I. Blaga, A. D. DiChiara, R. Santra, N. Berrah, C. Bostedt, J. D. Bozek, P. H. Bucksbaum *et al.*, Phys. Rev. Lett. **106**, 083002 (2011).
[9] H. Fukuzawa, S.-K. Son, K. Motomura, S. Mondal, K. Nagaya, S. Wada, X.-J. Liu, R. Feifel, T. Tachibana, Y. Ito *et al.*, Phys. Rev. Lett. **110**, 173005 (2013).
[10] L. Young, E. P. Kanter, B. Krässig, Y. Li, A. M. March, S. T. Pratt, R. Santra, S. H. Southworth, N. Rohringer, L. F. DiMauro *et al.*, Nature (London) **466**, 56 (2010).
[11] M. Klaiber, K. Z. Hatsagortsyan, and C. H. Keitel, Phys. Rev. A **71**, 033408 (2005).
[12] M. W. Walser, C. H. Keitel, A. Scrinzi, and T. Brabec, Phys. Rev. Lett. **85**, 5082 (2000).
[13] R. Mishra, D. Kalita, and A. Gupta, Eur. Phys. J. D **66**, 169 (2012).
[14] A. D. Bandrauk and H. Z. Lu, Phys. Rev. A **73**, 013412 (2006).
[15] N. J. Kylstra, R. A. Worthington, A. Patel, P. L. Knight, J. R. Vázquez de Aldana, and L. Roso, Phys. Rev. Lett. **85**, 1835 (2000).
[16] J. R. Vázquez de Aldana, N. J. Kylstra, L. Roso, P. L. Knight, A. Patel, and R. A. Worthington, Phys. Rev. A **64**, 013411 (2001).
[17] A. Bugacov, M. Pont, and R. Shakeshaft, Phys. Rev. A **48**, R4027 (1993).
[18] K. J. Meharg, J. S. Parker, and K. T. Taylor, J. Phys. B **38**, 237 (2005).
[19] M. Førre, S. Selstø, J. P. Hansen, and L. B. Madsen, Phys. Rev. Lett. **95**, 043601 (2005).
[20] M. Y. Emelin and M. Y. Ryabikin, Phys. Rev. A **89**, 013418 (2014).
[21] M. Gavrila, J. Phys. B **35**, R147 (2002).
[22] A. M. Popov, O. V. Tikhonova, and E. A. Volkova, J. Phys. B **36**, R125 (2003).
[23] M. Førre, J. P. Hansen, L. Kocbach, S. Selstø, and L. B. Madsen, Phys. Rev. Lett. **97**, 043601 (2006).
[24] M. Førre, Phys. Rev. A **74**, 065401 (2006).
[25] Z. Zhou and Shih-I. Chu, Phys. Rev. A **87**, 023407 (2013).
[26] M. Førre, S. Selstø, J. P. Hansen, T. K. Kjeldsen, and L. B. Madsen, Phys. Rev. A **76**, 033415 (2007).
[27] H. R. Varma, M. F. Ciappina, N. Rohringer, and R. Santra, Phys. Rev. A **80**, 053424 (2009).
[28] H. Bachau, M. Dondera, and V. Florescu, Phys. Rev. Lett. **112**, 073001 (2014).
[29] M. Dondera and H. Bachau, Phys. Rev. A **85**, 013423 (2012).
[30] V. Florescu, O. Budriga, and H. Bachau, Phys. Rev. A **86**, 033413 (2012).
[31] P. V. Demekhin, J. Phys. B **47**, 025602 (2014).
[32] E. Allaria, C. Callegari, D. Cocco, W. M. Fawley, M. Kiskinova, C. Masciovecchio, and F. Parmigiani, New J. Phys. **12**, 075002 (2010).
[33] C. I. Blaga, F. Catoire, P. Colosimo, G. G. Paulus, H. G. Muller, P. Agostini, and L. F. DiMauro, Nat. Phys. **5**, 335 (2009).
[34] W. Quan, Z. Lin, M. Wu, H. Kang, H. Liu, X. Liu, J. Chen, J. Liu, X. T. He, S. G. Chen *et al.*, Phys. Rev. Lett. **103**, 093001 (2009).
[35] F. Catoire, C. Blaga, E. Sistrunk, H. Muller, P. Agostini, and L. DiMauro, Laser Phys. **19**, 1574 (2009).
[36] K. Toyota, O. I. Tolstikhin, T. Morishita, and S. Watanabe, Phys. Rev. Lett. **103**, 153003 (2009).
[37] Y. I. Salamin, S. X. Hu, K. Z. Hatsagortsyan, and C. H. Keitel, Phys. Rep. **427**, 41 (2006).
[38] S. Selstø, E. Lindroth, and J. Bengtsson, Phys. Rev. A **79**, 043418 (2009).
[39] A. Di Piazza, C. Müller, K. Z. Hatsagortsyan, and C. H. Keitel, Rev. Mod. Phys. **84**, 1177 (2012).
[40] H. Bachau, E. Cormier, P. Decleva, J. E. Hansen, and F. Martín, Rep. Prog. Phys. **64**, 1815 (2001).
[41] E. Cormier and P. Lambropoulos, J. Phys. B **30**, 77 (1997).
[42] Y. Saad and M. H. Schultz, SIAM J. Sci. and Stat. Comput. **7**, 856 (1986).
[43] M. K. Gordon and L. F. Shampine, *Proceedings of the Annual Association for Computing Machinery Conference, 1974*, Vol. 1 (ACM, New York, 1974), pp. 46–53.